An Investigation of the Swirling Flow in a Spinning End-Burning Rocket

ROGER DUNLAP*
United Technology Center, Sunnyvale, Calif.

The purpose of this study was to determine the swirling flowfield which develops at various spin rates in the chamber of a spinning end-burning rocket. Cold flow experiments employing a porous plate to represent the propellant surface were conducted. The experiments were designed to simulate dynamically the conditions in a typical cylindrical rocket combustion chamber. Pressure measurements at the plate and in the flow were correlated with smoke traces to arrive at a physical description of the flowfield in which solid-body rotation gives way to a high-speed vortex in the chamber at sufficiently high motor spin rates. The experimental correlation of the onset of this flow transition with a critical value of the Rosby number is in agreement with a theoretical analysis, and it is concluded that the vortex development is a characteristic of the inviscid rotating flow. The experiments also indicate that significant interaction between the vortex and the propellant surface is little affected by chamber length or nozzle entrance shape.

Nomenclature

a_c = speed of sound in chamber
L_c = length of motor chamber
$\mathfrak{M}$ = molecular weight
P = pressure
P_c = chamber pressure
R = radius of motor chamber
r = radial coordinate
r_s = radial distance to smoke port
Re = Reynolds number
Ro = Rosby number, $Ro = U/2v_w$
T_c = temperature in chamber
u = radial velocity
U = axial velocity at propellant surface
v = tangential velocity
v_w = tangential velocity of chamber wall
w = axial velocity
Z = axial coordinate
μ = viscosity
ψ = stream function
ω,Ω = motor spin rate, flow rotation rate

Introduction

NUMEROUS tests have shown that spinning a solid propellant rocket about its longitudinal axis to promote flight stability may alter considerably its internal ballistics. The spinning rocket often exhibits a much higher rate of propellant consumption with an attendant increase in chamber pressure and reduction in burning time. Such spin-induced effects on solid rocket motor operation have been the subject of a number of recent investigations. Crowe[1] and Norton et al.[2] have presented comprehensive literature surveys of experimental and analytical work pertaining to this problem.

There are at least three different phenomena induced by spin which appear to have an effect on propellant burning: 1) centrifugal acceleration can directly affect the combustion process, 2) flow rotation affects the mass flow rate through the nozzle, and 3) vortex motion of the spinning chamber gases can cause erosive burning. The first of these effects has been demonstrated by studies conducted with centrifuges and with spinning internal-burning rocket motors.[1,3–7] Metallized propellants are found to exhibit large increases in burning rate when the centrifugal force acts perpendicularly into the propellant surface. High-speed motion pictures reported recently by Willoughby, Baker, and Crowe[1,8] show that under these conditions centrifugal force holds large metal oxide particles in pits which form on the surface. Increased heat transfer to the propellant beneath these particles is proposed as the mechanism by which the burning rate is increased.[1,8] As this mechanism would predict, the combustion process is not materially affected when the component of the centrifugal force normal to the propellant surface is small or zero. Thus in end-burning rockets no significant effect would be expected.

The effect of swirl of the propellant gases on mass flow rate through the nozzle has been analyzed for both a free vortex and solid-body rotation in the chamber representing the basic flow in internal burning cylindrical and end-burning grains, respectively. Mager's[9] analysis for the inviscid free vortex was extended by Norton et al.[10] to include viscous effects. The latter also analyzed the case of solid-body rotation and experimentally verified the predicted reduction in mass flow rate, using a cold flow apparatus to simulate both types of swirl. The studies show that an appreciable reduction in flow rate begins to occur when the tangential velocity at the grain surface becomes a few percent of the chamber sound speed. This leads to an increase in equilibrium chamber pressure and burning rate which can become significant at relatively high spin rates, particularly if the propellant has a low flame temperature and a high burning rate exponent.

The third effect of spin, with which this paper is concerned, results from the formation of a vortex in the chamber of end-burning rockets. At high spin rates an increased rate of propellant consumption is associated with the increased burning rate and surface area in a cone-shaped depression, or pit, which develops in the center of the propellant surface. This depression is presumably caused by erosive burning owing to vortex motion different from the solid-body rotation of the grain. However, the nature of such a vortex

Received February 14, 1969; revision received June 9, 1969. This research was supported by the Naval Ordnance Systems Command under Contracts NOw 66-0444-c and N00017-67-c-2429. The author would like to thank J. T. Lee and R. W. Hermsen for many useful suggestions and discussions. The contributions of P. G. Willoughby and L. F. Mahle in the design and execution of the experiments and of R. L. Carlson in the theoretical calculations are gratefully acknowledged.

* Senior Staff Scientist, Physical Sciences Laboratory. Member AIAA.

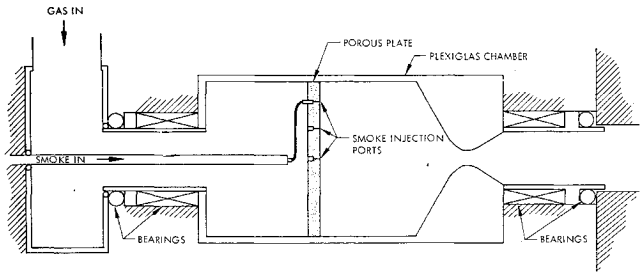

Fig. 1 Schematic diagram of simulated end-burner experiment.

flow and its dependence on spin rate and other rocket design parameters have not been determined.

The purpose of the investigation reported here was to examine the flow in the chamber of a spinning end burner with the aim of determining the swirling flow patterns which develop at various spin rates. Experimental measurements were used to arrive at a model of the flowfield and this model was compared with theoretical predictions. Because the environment which exists in an operating rocket motor chamber makes flow measurement and observation impractical, the flow was simulated in a cold flow apparatus employing a porous plate to represent the propellant grain. The requirements for dynamic simulation in this apparatus can be met with spin rates and chamber pressures much lower than those of the equivalent rocket. Pressure measurements at the plate and in the flow were correlated with smoke tracer observations to arrive at a model of the flowfield in which the solid-body rotation gives way to a high-speed vortex in the motor chamber at sufficiently high spin rates. Theoretical considerations for a steady, inviscid and incompressible flow indicate that the onset of this flow transition is governed by the ratio of the axial to the tangential velocities at the grain surface and this is in agreement with the experiments.

Flow Simulation

Two flows are dynamically similar when the governing equations in dimensionless form and appropriate boundary conditions are identical. Assuming steady and adiabatic flow of a gas with uniform composition in two geometrically similar spinning rocket motors, this condition is satisfied if both flows have the same Reynolds and Prandtl numbers, the same ratio of specific heats, and the same axial and tangential Mach numbers at the propellant surface. The last two parameters also imply that both flows have the same value of the Rosby number, $Ro = U/2\ v_w$ where U and v_w are the axial and tangential velocities at the propellant surface. Assuming that small differences in Prandtl number and specific heat ratio are of secondary importance in establishing the basic flow patterns of interest, and noting that the axial Mach number at the grain is essentially determined by the nozzle contraction ratio for choked flow, the main similarity parameters are the Reynolds number and either the ratio of spin velocity to chamber sound speed or the Rosby number. Equating these parameters for a rocket and a cold flow test in chambers with equal diameters gives the following relations for chamber pressure and spin rate:

$$\frac{(P_c)_{\text{cold flow}}}{(P_c)_{\text{rocket}}} = \frac{(a_c\mathfrak{M})_{\text{rocket}}}{(a_c\mathfrak{M})_{\text{cold flow}}} \frac{(T_c\mu_c)_{\text{cold flow}}}{(T_c\mu_c)_{\text{rocket}}} \tag{1}$$

$$\frac{(\omega)_{\text{cold flow}}}{(\omega)_{\text{rocket}}} = \frac{(a_c)_{\text{cold flow}}}{(a_c)_{\text{rocket}}} \tag{2}$$

where ω is the spin rate and subscript c refers to chamber conditions. If room temperature nitrogen is used in the cold flow test and a typical solid propellant rocket with $a_c = 13 \times 10^4$ cm/sec (4260 fps) and $\mu_c = 7 \times 10^{-4}$ g/cm-sec is to be simulated, then

$$(P_c)_{\text{cold flow}} = 0.065\ (P_c)_{\text{rocket}} \tag{3}$$

$$(\omega)_{\text{cold flow}} = 0.25\ (\omega)_{\text{rocket}} \tag{4}$$

Thus, the cold flow apparatus running at a chamber pressure of 65 psia and a spin rate of 3000 rpm simulates a rocket at 1000 psia and 12,000 rpm.

Experimental Apparatus

Experimental Setup

On the basis of the preceding, a cold flow spin motor was designed and constructed to operate at chamber pressures up to 130 psia and spin rates up to 4000 rpm. A schematic diagram is shown in Fig. 1. The end-burning surface was simulated by a $\frac{1}{8}$-in.-thick stainless steel porous plate. The plexiglas chamber had a 3.48-in. inside diameter and, for most of the tests, was connected to a nozzle with a 45° entrance cone and a 0.286-in.-diam throat. The distance between the porous plate and the nozzle entrance was 1.0 and 4.0 in. for the two chambers used with this nozzle. Other chamber-nozzle configurations are described later, together with the results. The chamber, porous plate, and nozzle rotate as a unit, and are driven by a belt from a $\frac{1}{2}$-hp variable-speed constant-torque electric motor.

Nitrogen gas is supplied from a cascade at 2200 psi and regulated to the desired chamber pressure. For upstream chamber pressures of 30 to 85 psia the pressure drop across the porous plate was found to vary from 9.5 to 14.4 psi. A pressure drop of this magnitude tends to isolate the upstream side of the porous plate from small radial pressure gradients which develop on the downstream side of the plate.

Pressure measurements in the flow and on the plate were taken with a probe connected to a central tube which spins with the motor and exits through an O-ring seal into a stationary chamber. The pressure in the chamber is read with a precision bourdon gage. The same passageway was used for the injection of titanium tetrachloride vapor into the flow. The streamline patterns were then observed with the aid of a stroboscopic light which was triggered and synchronized by light reflected from a spot on the spinning motor. By using a variable time delay unit a stationary view of the gas flow is obtained at any desired angular position of the motor.

Smoke Generation

The smoke generating scheme employed titanium tetrachloride which reacts with water at room temperature to produce a smoke consisting of solid titanium dioxide particles and hydrogen chloride. To avoid the problem of clogging feed pipes and valves, the titanium tetrachloride and water were ducted separately into the motor chamber. The water was atomized into the nitrogen main flow which had been heated to about 100°F to insure adequate water content at the operating pressures. The titanium tetrachloride was picked up as a vapor by dry nitrogen and introduced through the smoke port (Fig. 1); the liquid was heated to temperatures as high as 150°F to obtain the desired concentration in the carrier gas. This technique was found to be trouble-free and dependable, and produced controlled smoke flow rates on demand at varying chamber pressures.

Experiments and Results

Essentially four different experiments were performed to determine the effects of spin on the nature of the swirling flow in the rocket chamber. First were preliminary tests with a small sphere placed in the flow whose deflection indi-

cated the presence of a vortex at the plate at sufficiently high spin rates. Secondly, Pitot and static pressures were measured at the plate to define quantitatively the vortex flow. Thirdly, visual tests were made with smoke tracers which showed the transition from solid body rotation at low spin rates to a vortex motion at high spin rates, and indicated the presence of flow separation in the chamber. Finally, the effects of Reynolds number, nozzle contraction ratio, and chamber geometry on vortex formation were examined using the wall and centerline pressures at the plate as an indication of the rotational nature of the flow.

Preliminary Visual Observations

To verify the existence of a vortex near the surface of the porous plate at high spin rates, a simple test was performed. A small metal tee was fastened to the center of the plate, a string was attached to its top and a 0.090-in.-diam hollow sphere was attached to the end of the string. The plate was located 1 in. from the nozzle entrance; the ball was located $\frac{1}{4}$ in. above the plate and $\frac{1}{2}$ in. out from the center. At a chamber pressure of 28 psia and spin rates below 1000 rpm the string stretched radially outward from the supporting top of the tee due to the centrifugal force on the ball. However, at higher spin rates the ball and string were deflected in the direction of spin by the relative swirl motion through angles up to about 35° at 3200 rpm. By equating the drag and centrifugal components of force perpendicular to the string it was possible to estimate the drag and thus the swirl velocity. These calculations indicated swirl velocities relative to the plate as high as 200 fps. In a similar experiment at a chamber pressure of 65 psia the ball and string exceeded the maximum stable deflection and began to rotate, indicating a swirl velocity of over 260 fps. These observations, although only qualitative due to uncertainties in the sphere drag coefficient in this nonuniform flowfield, show that the flow near the centerline is spinning an order of magnitude faster than the motor at high motor spin rates.

Pressure and Velocity Measurements at Plate

Measurements were made of the static pressure on the surface of the porous plate and of the total pressure $\frac{1}{4}$ in. above the plate at various spin rates from 0 to 3280 rpm. Pitot probes were inserted through the chamber wall and connected to the central exit tube leading from the motor (Fig. 1). They were shaped so that the opening was perpendicular to a

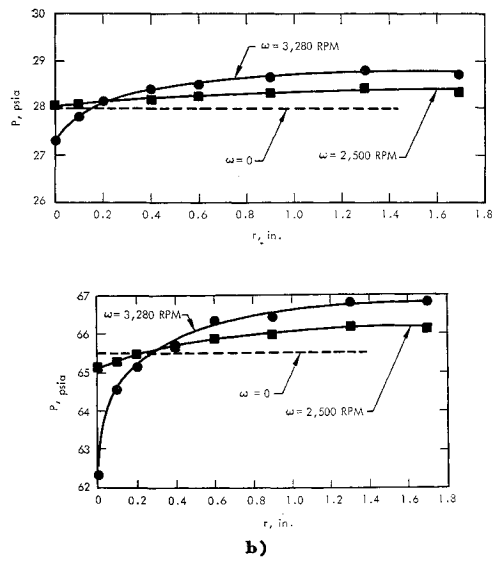

Fig. 2 a) Radial pressure distribution on plate — $P_{\omega=0}$ = 28.0 psia. b) radial pressure distribution on plate — $P_{\omega=0}$ = 65.5 psia.

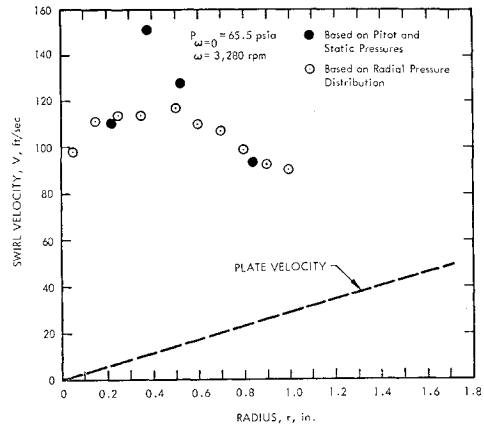

Fig. 3 Swirl velocity distribution above plate — $P_{\omega=0}$ = 65.5 psia, ω = 3280 rpm.

radius and thus measured total pressure when the velocity vector was essentially in the swirl direction. The static pressure probes were inserted through holes drilled in the plate.

The pressure upstream of the porous plate and the probe measurement were read simultaneously so that variations in regulator pressure could be accounted for. As the motor was spun faster the mass flow rate decreased slightly and this caused a small change in upstream pressure due to the regulator characteristics. All pressure measurements were corrected to the same value of upstream chamber pressure, assuming the pressure drop across the porous plate for a given upstream pressure was the same whether it was rotating or stationary.

The radial pressure distribution on the porous plate is shown in Figs. 2a and 2b for pressure levels of 28 and 65.5 psia. If the flow in the chamber were rotating as a solid body in unison with the plate, the pressure difference between the wall and centerline would be less than 0.10 psi at the highest spin rate and pressure level; this is negligible compared to the radial pressure differences which were found to exist. Thus, the pressure distributions indicate that at high motor spin rates there is a radial inflow and accompanying increase in swirl velocity. The larger pressure gradients are required to balance increased centrifugal accelerations. The radial pressure distribution was found to start changing rapidly when the motor spin rate was increased above 2000 rpm, indicating the presence of a vortex of rapidly increasing strength, in agreement with the visual observations described previously.

The Pitot pressure distribution $\frac{1}{4}$ in. above the plate was measured for the same pressure levels as those in Fig. 2. The total pressure was found to increase slightly with radius and spin rate. On the basis of the pressure measurements, an estimate was made of the swirl velocity above the plate. This was done in two ways. First, Bernoullis' equation can be used to calculate the velocity if it is assumed that the static pressure measured on the plate is the same as that $\frac{1}{4}$ in. above the plate where the total pressure was measured, and that the velocity vector is essentially in the swirl direction.† Secondly, the swirl velocity may be calculated from the radial pressure gradient if radial accelerations are assumed negligible compared to the centrifugal accelerations. The results of these two calculations are shown in Fig. 3 for the highest spin rate. The two methods show reasonable agreement except near the center of the plate where radial flow accelerations may be important and the pressure gradient method therefore in error. The vortex above the plate has

† The axial velocity at the plate is only 4.2 fps, so that the velocity vector was expected to be essentially in the swirl direction at high spin rates.

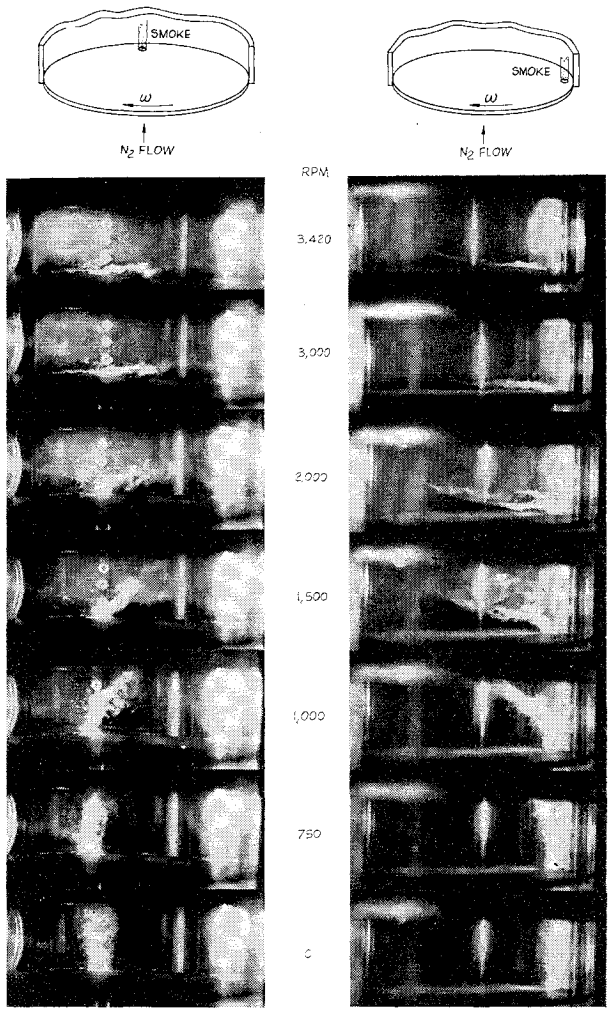

Fig. 4 Photographs of smoke tracer in simulated spinning end-burner; P_c = 28.7 psia, L_c = 1 in., r_s = 1.45 in.

rotational rates an order of magnitude greater than the motor spin rate, and would promote erosive burning when in contact with a propellant grain. The width of the region of high relative swirl velocities is seen to be an appreciable fraction of the chamber diameter.‡

Smoke Tracer Experiments

To study the nature of the vortex development at high spin rates three series of experiments were performed using smoke tracers. The smoke was injected through a hole in the porous plate and photographs were taken of the resulting smoke patterns. A Stroboslave light source was synchronized to the spin rate by a photoelectric pickup which receives a signal from a reflecting spot on the motor case. A single 3 μ sec flash with an intensity of 18 $\times$ 10^6 beam candles was sufficient to obtain good exposure with Polaroid ASA 3000 film.

In the first test series, the porous plate was located 1 in. from the nozzle entrance, simulating the case when the end-burning surface has not burned back appreciably. The smoke port was located 1.45 in. radially from the center of the plate which was 1.75 in. in radius. The results of the experiments are shown in Fig. 4 as a series of photographs taken at increasing spin rates. The smoke was photographed from two angles as indicated in the figure. The pictures show the transition from a solid-body flow in the chamber at low rpm, moving in unison with the plate, to an entirely different flow pattern at high rpm in which the flow issuing through the porous plate is accelerated radially inward across the surface and then turns up and spirals toward the nozzle. (This upward spiral is faintly visible in the top two right-hand photos.) The radially inward motion provides the mechanism for the high relative swirl velocities found in the earlier experiments, i.e., the swirl velocity on a streamline just outside the boundary layer at the plate increases inversely with radius to conserve angular momentum. From the pictures, the flow transition appears to take place near the plate between 1000 and 2000 rpm. Above 2000 rpm the flow moves mostly radially and circumferentially across the plate and below 1000 rpm it moves perpendicularly away from the plate.

In the second and third test series the porous plate was located 4 in. from the nozzle entrance. Results of the second test series, in which the smoke port was again located 1.45 in. from the center of the plate, are presented in Fig. 5. As the spin rate was increased to 1000 rpm the smoke plume began to behave as it had in the shorter chamber, i.e., it started to bend radially inward and in the direction of rotation. However, at higher spin rates, 1500 and 2000 rpm, the flow differed from that in the shorter chamber. The smoke is seen to break up and become diffuse, forming a cloud near the walls of the chamber. The density of the cloud over a large area indicates that some smoke is accumulating in the chamber rather than flowing out through the nozzle.§ This indicates a rather large region of flow separation near the chamber walls, which would be expected if a major part of the flow issuing through the plate moves radially inward near the plate.

To determine if the flow near the plate and closer to the centerline was similar to that in the shorter chamber, the smoke port was moved radially inward to a location 1.15 in. from the centerline. The results of this third test series are presented in Fig. 6. It is seen that the smoke behaves essentially as in the first test series with the shorter chamber (Fig. 4), moving radially inward and spinning faster than the plate at high motor spin rates. A particularly interesting result is shown in the photograph at 2000 rpm in which the smoke jet broke up into two distinct parts. The lower part

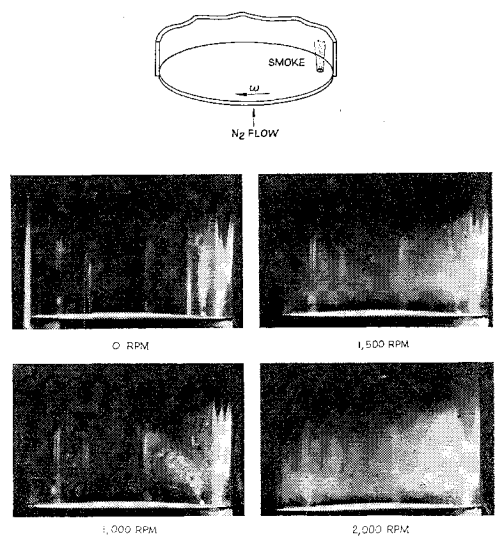

Fig. 5 Photographs of smoke tracer in simulated spinning end-burner; P_c = 28.7 psia, L_c = 4 in., r_s = 1.45 in.

‡ Recent measurements reported in Ref. 14 also show similar increases in swirl velocity at high spin rates.

§ The smoke injection velocity was 30 fps compared to an axial flow velocity from the plate of 4.2 fps without spin. Thus, there is a tendency for the smoke to penetrate across main flow streamlines in regions of low velocity.

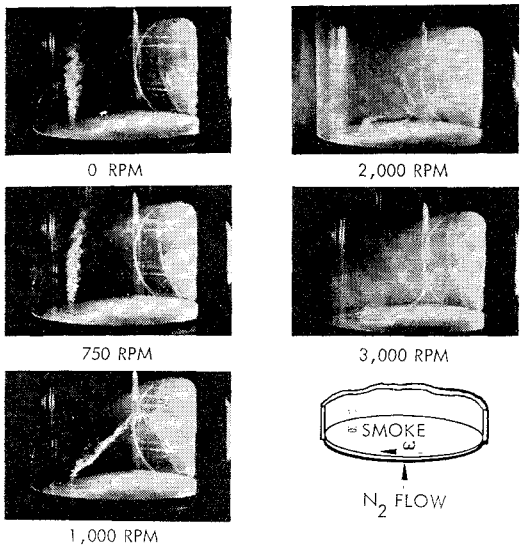

Fig. 6 Photographs of smoke tracer in simulated spinning end-burner; P_c = 28.7 psia, L_c = 4 in., r_s = 1.15 in.

near the plate accelerated radially inward and spiraled up the center, whereas the outer part of the jet was influenced more by the swirl motion and moved mostly in the spin direction. This indicates that strong gradients in radial and swirl velocities exist near the plate surface.

On the basis of the smoke injection experiments, a qualitative picture of the flowfield at high spin rates is shown in Fig. 7. Since the flow moves radially inward close to the plate, there exists a large separated region near the chamber walls, as indicated by the smoke tests of Fig. 5. The radial inflow near the plate is the mechanism for the high swirl velocities above the plate since the swirl velocity increases inversely with the radius to conserve angular momentum (neglecting viscous effects very near the plate).

Effect of Geometry, Reynolds Number, and Nozzle Contraction Ratio

A final series of experiments was performed to investigate the effect of chamber geometry, Reynolds number, and nozzle contraction ratio on the transition to a vortex in the rocket chamber. As discussed in the next section, if viscous and compressible effects are of secondary importance, the rotational character of the flow should depend only on the ratio of

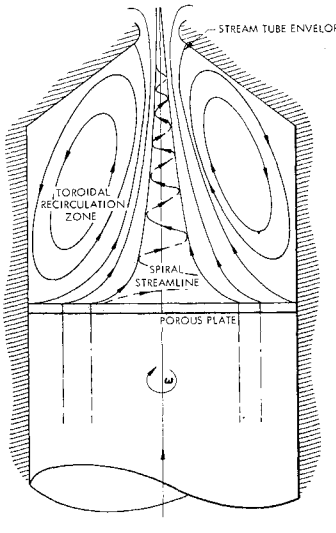

Fig. 7 Model of flowfield at high motor spin rates.

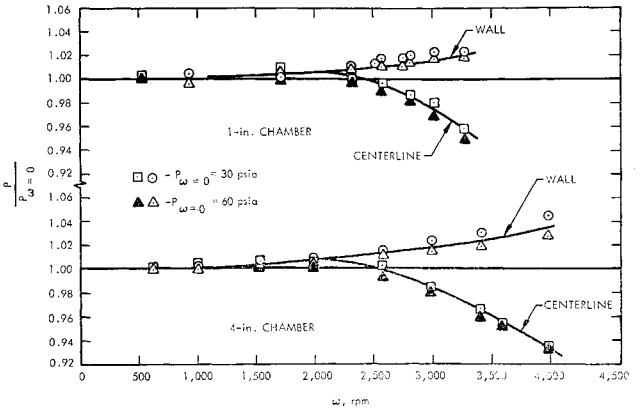

Fig. 8 Effect of chamber length and chamber pressure on plate static pressure vs spin rate, U = 4.2 fps.

axial-to-spin velocities, or the Rosby number, $Ro = U/2v_w$. Thus, in the tests with different contraction ratios and hence different axial velocities at the porous plate, it was of particular interest to establish whether vortex formation occurred at a single value of Rosby number.

As mentioned previously, the wall and centerline pressures on the porous plate would differ only to a negligible extent at the pressures and spin rates used in these tests as long as the flow remains in solid-body rotation at the plate. The development of the vortex motion was characterized by a rapidly increasing difference between these two pressures. Pressure measurements therefore serve as a simple method of detecting gross changes in the rotational nature of the flow with increasing spin rate and were so used in this test series.

Typical pressure vs spin rate data are shown in Fig. 8 for the 1-in. and 4-in. long straight chambers, at two chamber pressure levels. For all conditions the wall and centerline pressures are seen to separate at approximately 2000 rpm. Comparison with the smoke photographs of Fig. 4 shows the nature of the flow near the plate at this spin rate to be completely changed from the solid-body motion. Beyond this spin rate significant interaction of the vortex with the plate probably occurs, in accordance with the pressure differences measured. There is essentially no effect of the fourfold increase in chamber length or the twofold increase in Reynolds number on the behavior of wall and centerline pressures with spin rate.

The influence of chamber and nozzle shape on the vortex flows was examined for several different geometries, as shown in Fig. 9. The data show little effect of the three shape changes on the separation of wall and centerline pressures

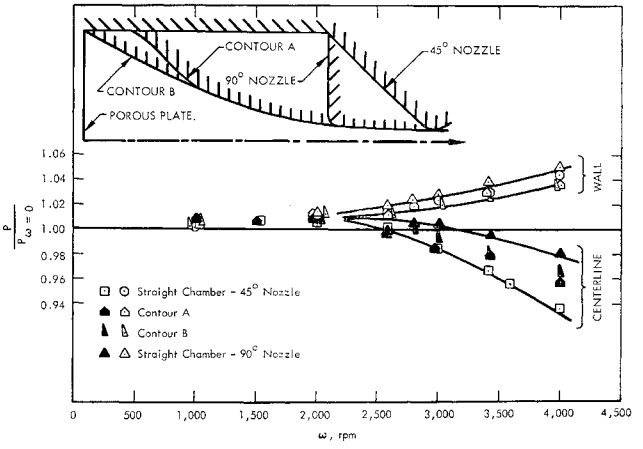

Fig. 9 Effect of chamber geometry on plate static pressure vs spin rate, $P_{\omega=0}$ = 28 psia.

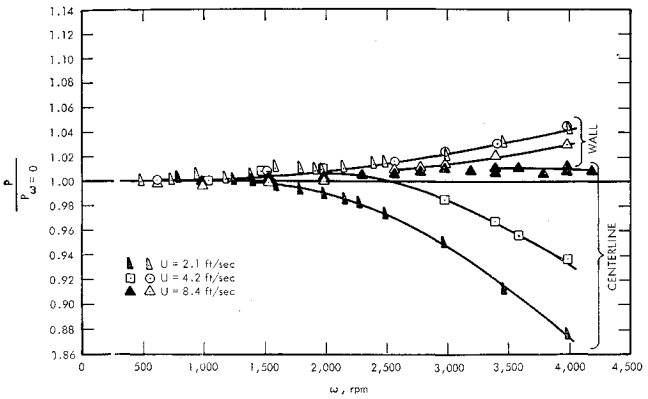

Fig. 10 Effect of axial velocity in chamber on plate static pressure vs spin rate, L_c = 4 in., $P_{\omega=0}$ = 28 psia.

which still occurs at about 2000 rpm. The vortex formation has apparently not been delayed by the changes in geometry.

Finally, the contraction ratio of the 45° nozzle was both increased and decreased by changing the throat diameter. The corresponding axial velocities at the plate were 2.1, 4.2, and 8.4 fps, giving a fourfold change in Rosby number at each spin rate. The pressure data are shown in Fig. 10. It can be seen that the vortex occurs at lower rpm with the lower axial velocity and at higher rpm with the higher axial velocity. The wall and centerline pressures at U = 8.4 fps begin to separate between 3000 and 4000 rpm and the shape of the centerline pressure is still relatively flat at 4000 rpm. A distinct pressure difference occurs at about 1000 and 2000 rpm for U = 2.1 and 4.2 fps, respectively. Thus, significant vortex interaction with the plate appears to correlate with the Rosby number in the flow. Choosing 1000, 2000, and 3500 as the critical spin rates for the three axial velocities, the corresponding Rosby numbers are 0.07, 0.07, and 0.08, respectively. For higher values of the Rosby number there would not appear to be a significant effect of spin on the flow at the surface of the plate. However, the flow above the plate begins to change at higher Rosby numbers as shown in the smoke studies and discussed further below.

Theory and Discussion

The literature reveals a large number of analyses devoted to various aspects of vortex motion. Several very good survey articles are presented in Ref. 11. In 1956, Long[12] presented a solution for an inviscid and incompressible fluid which has uniform axial velocity and solid-body rotation far upstream, and flows into a sink on the axis of the otherwise closed end of a round tube. This flow situation contains the essential features of the present experiment and, as discussed below, the solution provides a basis for understanding the initial stages of the vortex transition which was observed.

Equation for the Stream Function

Neglecting viscous and compressible effects, the angular momentum and total pressure are constant on streamlines and the equations for conservation of mass and momentum may be reduced to an equation for the stream function.[1,13] Assuming axial symmetry and specifying that the flow has uniform axial velocity U and solid-body rotation Ω, at an upstream boundary of the flow, the equation for the stream function may be written in dimensionless form as

$$\frac{\partial^2\psi'}{\partial Z'^2} + \frac{\partial^2\psi'}{\partial r'^2} - \frac{1}{r'}\frac{\partial\psi'}{\partial r'} + R_0^{-2}(\psi' - r'^2) = 0 \qquad (5)$$

where

$$\psi' = \frac{\psi}{\psi_{\text{wall}}},\ Z' = \frac{Z}{R},\ r' = \frac{r}{R},\ R_0 = \frac{U}{2\Omega R} \qquad (6)$$

and R is the radius of the outer streamline at the upstream boundary. The radial, axial, and swirl velocities are derived from the stream function according to the relations

$$\begin{aligned} u' &= u/U = -(1/2r')(\partial\psi'/\partial Z') \\ w' &= w/U = (1/2r')(\partial\psi'/\partial r') \\ v' &= v/U = (1/2R_0)(\psi'/r') \end{aligned} \qquad (7)$$

The desired solution of Eq. (5) is that for which $\psi' = 1$ along the chamber and nozzle walls and the upstream boundary condition is maintained at a fixed axial position (porous plate or propellant surface). In general a numerical procedure is required to determine the stream function for an arbitrary geometry. Solutions in terms of infinite series were found when the centerline velocity was prescribed and the geometry left unspecified, but these were difficult to interpret in terms of the effect of spin since both geometry and spin rate varied at the same time.[1]

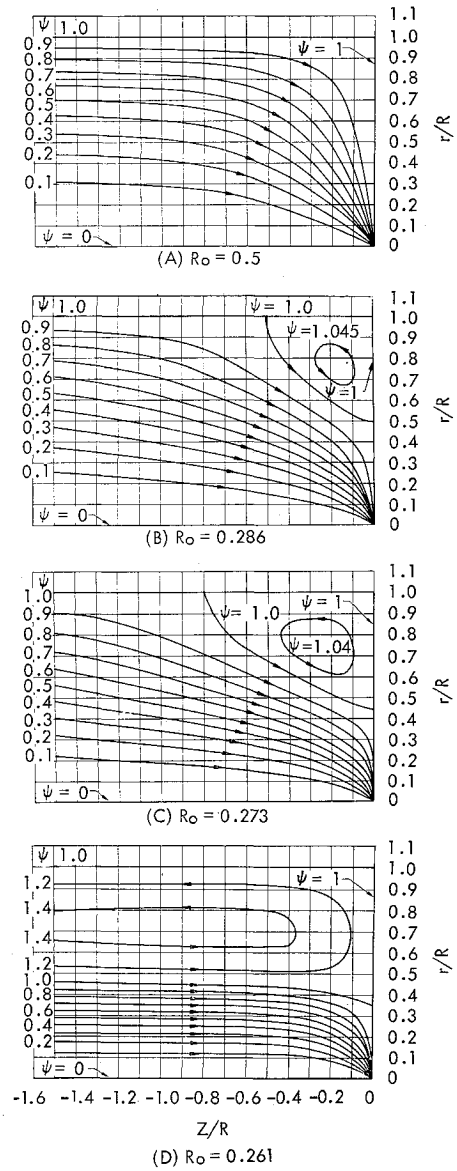

Fig. 11 Streamline envelopes for swirling flow into a sink; a) R_0 = 0.50; b) R_0 = 0.286; c) R_0 = 0.273; d) R_0 = 0.261.

Flow into a Sink

A solution to Eq. (5) was presented by Long[12] for the case of flow in a round tube where the fluid starts at $Z = -\infty$ and flows into a sink on the axis at $Z = 0$ where the tube terminates in a vertical wall. This flow contains the essential features of the spinning rocket in that it starts in solid body rotation and then converges toward the centerline. In terms of the present notation Long's solution is

$$\psi' = r'^2 + 2r' \sum_{n=1}^{\infty} \frac{\exp[(Z_n^2 - R_0^{-2})^{1/2} Z']}{Z_n J_0^2(Z_n)} J_1(Z_n r') \quad (8)$$

where J_0 and J_1 are the zero- and first-order Bessel functions of the first kind and the Z_n are the successive zeros of J_1. As shown by Long, this solution predicts flow separation as the Rosby number approaches the value 0.261, and is not valid for $R_0 < 0.261$ because the boundary condition at $Z = -\infty$ cannot be maintained. The flow patterns were calculated for several values of the Rosby number and are shown in Fig. 11. The separated region appears in the corner for $R_0 = 0.286$ and increases rapidly as R_0 is decreased to the critical value of 0.261. At the critical spin rate, given by $\Omega R = 1.92\ U$, the separated region has extended back to $-\infty$ and the sink flow is drawn only through the central portion of the tube.

Discussion

The preceding development of flow separation, and the attendant increase in swirl velocity as the streamlines converge closer to the centerline, are in qualitative agreement with the results of the present experiments. The occurrence of this change in the flow at a critical Rosby number is also in general agreement with the experimental results. For the experimental conditions of the smoke photographs in Fig. 4 the Rosby number decreased to 0.261 at a spin rate of about 550 rpm. Changes in the smoke pattern above the plate are evident at 750 and 1000 rpm, and the flow at the plate began to show a significant radial pressure gradient above 2000 rpm (Fig. 8). Considering that the porous plate inhibits the large change in flow suggested by the aforementioned theory as the spin rate approaches 550 rpm, the fact that the flow does begin to change from solid-body motion near this spin rate indicates that the initial stage of the vortex development is a characteristic of the inviscid flow and is governed by a critical Rosby number. The way in which the flow continues to change as the Rosby number is decreased below the critical value requires further analysis using the correct upstream boundary condition. Viscous effects will also be important in the vicinity of the plate at high spin rates.

Further Comparison of Theory and Experiment

To more quantitatively relate the vortex development to the inviscid flow behavior discussed earlier, the centerline velocity near the chamber exit was measured as a function of spin rate and compared with that derived from Eq. (8). This comparison is shown in Fig. 12. The theory shows a rapid increase in velocity as the Rosby number approaches 0.261, and the experiments show that a somewhat slower increase in velocity begins to occur in the same region of spin rates. Although the presence of the porous plate modifies the rapid change in velocity predicted for the sink flow, the experimental results confirm that the onset of the flow transition is governed by the same critical value of the Rosby number.

Summary and Conclusions

Experiments performed under conditions which simulate those in a spinning end-burning rocket motor show that the swirling flow in the rocket chamber has the following characteristics.

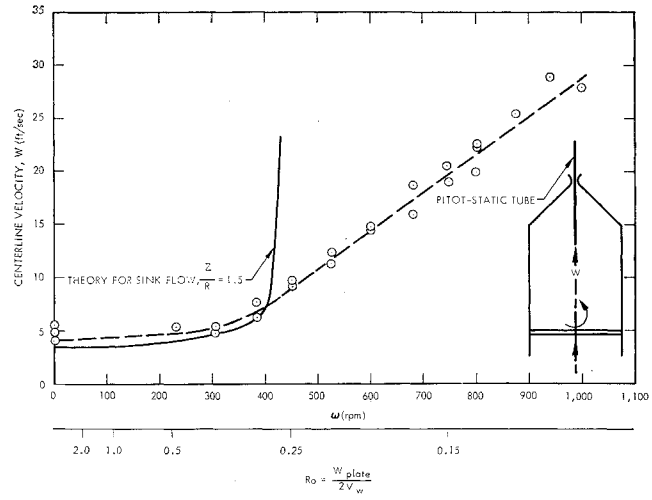

Fig. 12 Centerline velocity near chamber exit vs spin rate.

1) At low motor spin rates the flow is in solid-body rotation in unison with the simulated propellant surface.

2) When the spin rate exceeds a critical value flow separation begins to occur in the downstream regions of the chamber and the main flow moves toward the centerline.

3) At very high motor spin rates a large portion of the flow moves radially inward across the "propellant" surface and spirals out the central portion of the chamber. This results in a large recirculation zone in the chamber and a vortex adjacent to the propellant which has spin rates an order of magnitude greater than the motor.

Correlation of the onset of the flow transition with a critical Rosby number of 0.261 is consistent with experimental observations and with theoretical predictions for inviscid and incompressible flow. As the Rosby number was decreased to a value of 0.07 the strength of the vortex was sufficient to produce a noticeable pressure gradient at the "propellant" surface.

Using the pressure difference between the center and the edge of the simulated propellant surface to indicate the presence of significant vortex development near the surface, experiments showed that: 1) there was little effect of changes in nozzle geometry and chamber length on the vortex development; 2) no effect of Reynolds number was found over a two-fold range; and 3) the vortex occurred at nearly the same Rosby number when the nozzle contraction ratio was varied. The results of this study provide an explanation for the propellant erosion found in spinning end-burning rockets and suggest that this effect will not occur in motor configurations designed to ensure a sufficiently high Rosby number in the combustion chamber.

References

[1] Willoughby, P. G. et al., "Investigation of Internal Ballistic Effects in Spinning Solid Propellant Motors," UTC 2281-FR, Oct. 1968, United Technology Center, Sunnyvale, Calif.

[2] Norton, D. J., Farquhar, B. W., and Hoffman, J. D., "Analytical Studies of the Interior Ballistics of Spinning Rocket Motors—A Literature Survey," TM-67-1, Jan. 1967, Jet Propulsion Center, Purdue Univ., Lafayette, Ind.

[3] Burchard, J. K. et al., "Investigation of Performance Losses and Ballistic Effects in Solid Propellant Rockets," UTC 2197-FR, April 1967, United Technology Center, Sunnyvale, Calif.

[4] Crowe, C. T. et al., "Investigation of Particle Growth and Ballistic Effects on Solid Propellant Rockets," UTC 2128-FR, June 1966, United Technology Center, Sunnyvale, Calif.

[5] Anderson, J. B. and Reichenbach, R. E., "An Investigation of the Effect of Acceleration on the Burning Rate of Composite Propellants," *AIAA Journal*, Vol. 6, No. 2, Feb. 1968, pp. 271–277.

[6] Sturm, E. J. and Reichenbach, R. E., "An Experimental

Study of the Burning Rates of Aluminized Composite Propellants in Acceleration Fields," AIAA Paper 68-529, Atlantic City, N.J., June 1968.

[7] Northam, G. B. and Lucy, M. H., "On the Effects of Acceleration Upon Solid Rocket Performance," presented at the Third ICRPG/AIAA Solid Propulsion Conference, Atlantic City, N.J., June 1968.

[8] Willoughby, P. G., Baker, K. L., and Crowe, C. T., "A Photographic and Analytic Study of Composite Propellant Combustion in an Acceleration Field," AIAA Paper 69-173, New York, 1969.

[9] Mager, A., "Approximate Solution of Isentropic Swirling Flow Through a Nozzle," *ARS Journal*, Vol. 31, No. 8, Aug. 1961, pp. 1140–1148.

[10] Norton, D. J., Farquhar, B. W., and Hoffman, J. D., "An Analytical and Experimental Investigation of Swirling Flow in Nozzles," F-67-9, Oct. 1697, Jet Propulsion Center, Purdue Univ., Lafayette, Ind.

[11] Küchemann, D., *Progress in Aeronautical Sciences, Volume 7*, 1st ed., Pergamon Press, Oxford, 1966.

[12] Long, R. R., "Sources and Sinks at the Axis of a Rotating Liquid," *Quarterly Journal of Mechanics and Applied Mathematics*, Vol. IX, Pt. 4, 1956, pp. 385–393.

[13] Batchelor, G. K., *An Introduction to Fluid Dynamics*, Cambridge Univ. Press, 1967.

[14] Johnson, G. R. and L'Ecuyer, M. R., "An Experimental Investigation of the Pressure and Velocity Profiles in a Spinning, Cold-Flow Rocket Motor," TM-68-6, August 1968, Jet Propulsion Center, Purdue Univ., Lafayette, Ind.

DECEMBER 1969 AIAA JOURNAL VOL. 7, NO. 12

Onset of Instabilities in Coaxial Hall Current Accelerators

H. A. Hassan* and Charles C. Thompson†
North Carolina State University, Raleigh, N.C.

An analysis is presented with the objective of predicting the onset of spokes in MPD arcs. A simple geometry consisting of coaxial electrodes with applied radial electric field and axial magnetic field is investigated with the analysis being based upon the ion and electron conservation equations. After obtaining a steady-state solution that takes into consideration the existence of anode and cathode sheaths, an $m = 1$ helical perturbation is analyzed using a normal mode analysis. The results indicate that the critical magnetic field increases with pressure, and because of the geometry chosen, it is independent of the current. The instability is of the Simon-Hoh type.

Introduction

EXPERIMENTS at various laboratories[1–4] indicate that, under certain operating conditions, the arc current in an MPD thruster tends to concentrate into a rotating spoke. This form of instability rotates in the $\mathbf{E} \times \mathbf{B}$ direction with an angular velocity that increases with magnetic field strength and current but decreases with mass flow rate. More recent experiments[5,6] indicate that the formation of the spoke is associated with an onset with the critical magnetic field being of the order of a few hundred gauss.

The object of this investigation is to determine the onset of instabilities in MPD arcs. The usual procedure employed in studies of this nature is to obtain a steady-state solution of the governing equations that are assumed to be the conservation equations for the ions and electrons. A perturbation is then superimposed on the system; if it does not grow with time the system is stable, otherwise it is unstable. There are at least two major complications associated with such a procedure for the problem under consideration. The complexity of the geometry makes it impossible to obtain an analytical solution. In addition, even when a simple geometry is assumed, one cannot ignore the anode and cathode sheaths as is normally done in the study of similar problems for the positive column,[7] or the linear Hall current accelerator.[8]

In this work, a simple geometry consisting of an inner cathode and an outer ring anode combined with an axial magnetic field (Fig. 1) is employed. The electric and magnetic field arrangement considered here is similar to that discussed by Hoh[9] for a Penning discharge. The analysis presented here differs from that of Ref. 9 in that a steady-state solution that takes into consideration the existence of anode and cathode sheaths has been obtained, and a normal mode analysis instead of dimensional analysis is used to analyze the instability.

The governing equations are the usual conservation of mass and momentum for ions and electrons. The inertia terms in the ion and electron momentum equations are usually ignored and this assumption has been made here. Although one is justified in ignoring the electron inertia terms, neglect of the ion inertia terms requires further justification. A partial justification follows from the work of Persson[10] on the positive column where it is shown that linear ambipolar diffusion gives a fairly good approximation of the steady-state solution if the ambipolar velocity is less than the speed of sound of the ion-electron pair. This, coupled with the fact that for the problem under consideration, the radial ion current is much less than the radial electron current, indicates that neglecting the ion inertia terms is justified provided one uses appropriate boundary conditions.

Using a procedure similar to that employed for the positive column, the appropriate boundary conditions at the edge of the cathode sheath can be inferred from investigation of the singular points of the complete differential equations. As is shown in Appendix A, the limiting velocity at the edge of the cathode sheath reduces to the speed of sound of the ion-electron pair when the net current is zero. The boundary condition at the edge of the anode sheath is obtained from the consideration that the current density is approximately equal to the random electron current density.

The steady-state solution obtained shows that the product of the radial component of the electric field and the density

Presented as Paper 69-230 at the AIAA 7th Electric Propulsion Conference, Williamsburg, Va., March 3–5, 1969; submitted February 19, 1969; revision received June 30, 1969. This work was supported, in part, by NASA Grant NGR 34-002-048.

* Professor of Mechanical and Aerospace Engineering. Associate Fellow AIAA.

† Research Assistant.